Tellus (1994), 46A, 75–85
Printed in Belgium – all rights reserved

TELLUS
ISSN 0280–6495

Geostrophic drag coefficients for the central Arctic derived from Soviet drifting station data*

By JAMES E. OVERLAND[1], *Pacific Marine Environmental Laboratory/NOAA, Seattle, WA 98115, USA*, and ROGER L. COLONY, *Polar Science Center, University of Washington, Seattle, WA 98195, USA*

(Manuscript received 13 July 1992; in final form 6 August 1993)

ABSTRACT

Based on 4 years of central arctic atmospheric sounding data and 10 years of surface wind data from Soviet drifting stations, combined with geostrophic winds from the arctic buoy program, the following relation between air-ice stress, τ, and the surface geostrophic wind speed, g, can be recommended

$\tau = \rho C_g^2 \gamma^2 g^2$,

$\rho C_g^2 = 0.85 \times 10^{-3}$ (nt m^{-2})(m^2 s^{-2})$^{-1}$,

$C_g = 0.024$, November–March,

$\rho C_g^2 = 1.10 \times 10^{-3}$ (nt m^{-2})(m^2 s^{-2})$^{-1}$,

$C_g = 0.029$, June–August.

If the spacing between sea level pressure values from buoys is greater than 400 km, such as in the arctic buoy array, a speed enhancement factor of $\gamma = 1.3$ should be applied to correct for insufficient sampling and smoothing in generating the geostrophic wind field. If the spacing is of order 100 km or less, then $\gamma = 1.0$. An inflow angle α, the angle between the geostrophic wind and the surface wind, of 33° is recommended for winter and 23° for summer. Values for the transition months April, May, September and October can be interpolated between winter and summer values. The winter value of C_g is calculated 3 ways: from the Soviet station surface wind-geostrophic wind speed ratio using suitable 10 m drag coefficients, from regression equations based on surface-900 mb stability, and from the AIDJEX analyses. The summer values are based on the surface wind-geostrophic wind ratio, model, and AIDJEX derived values. There is considerable day-to-day variability in atmospheric stability and geostrophic coefficients, but no statistically significant variation in the within-season monthly mean and median values; month-to-month variability is within 5% for C_g and 5° for α for the winter and summer seasons. Neglect of stability variations for daily cases can contribute an error of ± 40% in the relation between surface stress and geostrophic wind speed squared compared with using constant winter values. Use of atmospheric temperature profiles from satellites may increase the accuracy of C_g for daily cases by providing an estimate of lower-atmospheric inversion strength.

1. Introduction

Winds are the primary driving force for ice motion in the Arctic (Thorndike and Colony, 1982). Coupling of the air to the ice is given by geostrophic drag coefficient, the ratio of the friction velocity to the geostrophic wind speed

$$\tau = \rho C_g^2 g^2, \qquad C_g = u_*/g, \qquad u_*^2 \equiv \tau/\rho. \tag{1}$$

τ is the surface stress, C_g is the geostrophic drag

[1] Corresponding author.

* Contribution No. 1376 from NOAA/Pacific Marine Environmental Laboratory.

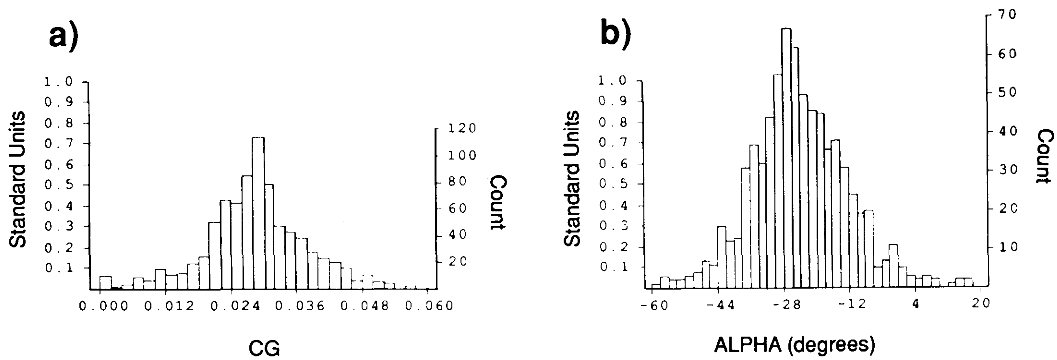

Fig. 1. (a) Distribution of geostrophic drag coefficient as measured northeast of Svalbard during the fall 1988 CEAREX drift. (b) Distribution of inflow angle between the surface and geostrophic wind for the CEAREX drift.

coefficient, u_* is the friction velocity, g the surface geostrophic wind speed derived from the sea-level pressure field, and ρ is air density. The inflow angle, α, is the change in direction between the surface stress and the geostrophic wind. In a recent paper, Overland and Davidson (1992) argue that the winter coupling of the air to the ice depends primarily on the atmospheric stability of the entire inversion layer from the surface to the base of the temperature maximum layer $\approx$900 mb, rather than on surface heat fluxes, i.e., Monin length (Doronin, 1969), or on the inversion strength just above the inversion base (Kitaigorodskii, 1988). This result is consistent with modeling results (Overland, 1985) that for the 7-month arctic winter season, the stratification of the boundary layer rather than surface roughness is the most important factor in the variability of C_g and α. These generalizations apply to the central Arctic and not necessarily to the seasonal ice zones.

Observations of C_g have been generally made over rather short periods of time. The observations reported by Overland and Davidson (1992) were for the fall CEAREX drift, October–December 1988 from the eastern Arctic northeast of Svalbard (Fig. 1). The question arises as to how repre-

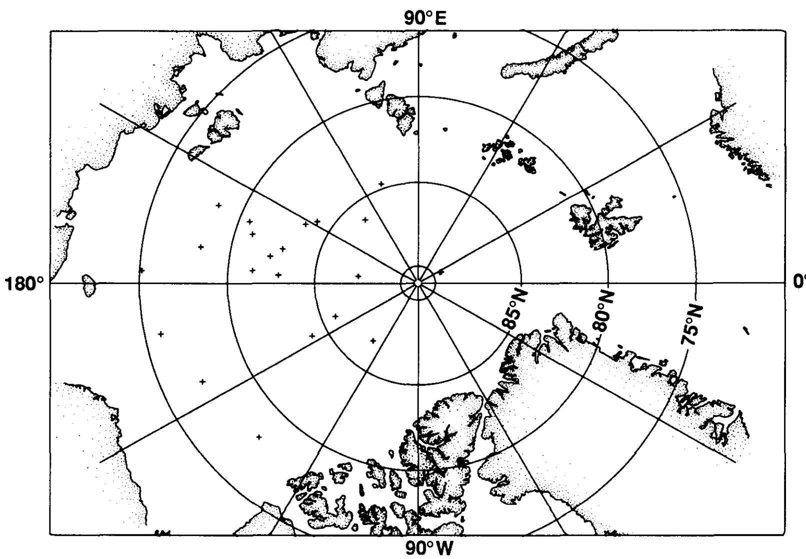

Fig. 2. Positions of Soviet drifting ice stations on 1 January for 1979–1990.

sentative the CEAREX values and the earlier AIDJEX values are to the entire Arctic and entire winter season. For example, aircraft measurements of two very stable central arctic cases for clear skies from March 1989 (Walter and Overland, 1991) had C_g values of almost half of the median CEAREX value, 0.015 compared to 0.029. These clear sky values fell at the extreme end of the distribution of the CEAREX data. Because C_g is squared to obtain the stress from the geostrophic wind, these C_g values imply almost a factor of 4 reduction in surface stress compared to using the median CEAREX value of C_g for the same geostrophic wind.

In this paper, we greatly expand the data base for C_g and α by calculating the monthly surface-geostrophic wind ratio and inflow angles from ten years of Soviet drifting station wind data and geostrophic wind data from the arctic buoy program. This data set is primarily from the western Arctic (Fig. 2). We relate this ratio to surface stress through assumptions on surface drag coefficient. Independently we make use of four years of atmospheric sounding data (almost 6 station years) from the Soviet drifting stations NP-22, NP-26 and NP-28 to establish the winter season distribution of stability for the western central Arctic. The regression equations developed in Overland and Davidson (1992) establish a median arctic C_g and inflow angle from the drifting station atmospheric boundary layer stability distribution. Comparisons between the methods are made and we suggest monthly values of C_g and α for use in driving sea-ice models from geostrophic winds. The possible errors in air-ice stress and surface wind direction calculated from geostrophic winds are estimated for the case when the boundary layer stability is not known.

2. The data sets

Surface wind data are from the Soviet "North Pole" series of drifting ice stations. Since 1950 the Soviets have operated 30 separate stations, collecting almost 80 station years of data. The format of the surface wind data has speed truncated to integer values of m s^{-1} and direction to the nearest 5°. The anemometers were mounted at 10 m. We use the period 1979–1990 (Fig. 2) which corresponds to the period of arctic buoy coverage (Colony and Rigor, 1991). A basinwide distribution of ARGOS buoys measuring surface pressure, separated by 500–600 km, was the goal of the arctic buoy program and typical analysis error for geostrophic wind near the center of the buoy network is about 2 m s^{-1} (Thorndike et al., 1983). Often there were two drifting stations operating at any one time and there are between 1178–1469 twice daily, paired surface wind-geostrophic wind observations per month.

The atmospheric sounding data are from NP-26 and NP-28, which are nearly complete for November 1983 through December 1987 except for March–June 1986 (Serreze et al., 1992), and from Station NP-22, which reported data from May 1979 through February 1982. The winter season sounding data (November–April, inclusive) are used and are limited to the period during which the stations were between 79°–90° N. This excludes data prior to 1981 from NP-22. With some missing data, this gave a total of 1532 soundings, rather complete winter coverage for the central Arctic, and 780 soundings for summer (June–August). Based on the mixture of sounding types and inspection of the monthly values of inflow and surface/geostrophic wind speed ratios, April, May, September and October can be considered transition months.

3. Wind statistics

The mean and variance of the vector surface wind, $w = (W_x, W_y)$, are defined by the expected value operator

$$E\{w\} = \bar{w} = (\bar{W}_x, \bar{W}_y)$$
$$E\{(w-\bar{w})(w-\bar{w})^{\mathrm{T}}\} = E\{(W_x-\bar{W}_x)^2 + (W_y-\bar{W}_y)^2\} = \mathrm{var}\{w\} = \sigma_w^2. \quad (2)$$

W_x is the component of wind directed parallel to the local latitude; W_y is directed parallel to the local longitude. The mean, $E\{G\}$, and variance, σ_G^2, of geostrophic wind are similarly defined. The mean vector wind averaged over all stations for a given month is small, typically less 1 m s^{-1}, although the magnitude of the mean annual vector geostrophic wind may be 2–3 m s^{-1} at a given location. The ensemble variance may be slightly larger than for equivalent fixed location winds because spatial patterns are incorporated into this definition of variance. The speed of the surface wind is defined as $s = |w| = [W_x^2 + W_y^2]^{1/2}$ and has mean and variance

$$E\{s\} = E\{|w|\} = E\{[W_x^2 + W_y^2]^{1/2}\} = \bar{s},$$
$$E\{(s-\bar{s})^2\} = \mathrm{var}\{s\} = \sigma_s^2. \tag{3}$$

As seen in eqs. (2) and (3), the standard deviation of vector wind is not the same as the mean wind speed. However, they take on similar values and either one may be regarded as a statistic for the monthly wind.

The mean and variance of W_x for 1361 January observations from 1979–1990 are 0.06 m s^{-1} and 20.0 m^2 s^{-2}. The distribution for W_y has a nearly equal mean and variance, -0.05 m s^{-1} and 20.0 m^2 s^{-2}. The correlation between W_x and W_y is not significantly different from zero. We conclude that the joint distribution is adequately approximated by an isotropic, zero mean, bivariate Gaussian distribution. Modeled wind speed, $z = (W_x^2 + W_y^2)^{1/2}$, will have Rayleigh distribution with mean, $\bar{z} = \sigma_w \pi^{1/2}/2 = 0.886\sigma_w$, and standard deviation, $\sigma_z = \sigma_w(4-\pi)^{1/2}/2 = 0.463\sigma_w$. For the January case, the Rayleigh distribution has mean and standard deviation, $\bar{z} = 5.6$ m s^{-1} and $\sigma_z = 2.9$ m s^{-1}, in agreement with the sample mean wind speed, $\bar{s} = 5.6$ m s^{-1}, and sample standard deviation $\sigma_s = 2.9$ m s^{-1} (Fig. 3). The most commonly observed wind speed, 5 m s^{-1}, can be compared to the mode of the Rayleigh distribution, $\sigma_w/2^{1/2} = 4.5$ m s^{-1}. The mean and variance for G_x in January was 0.03 m s^{-1} and 45.7 m^2 s^{-2}. For G_y, the values are -0.44 m s^{-1} and 46.8 m^2 s^{-2}. The modeled geostrophic wind speed, $0.886\sigma_G$, is 8.5 m s^{-1} compared to mean speed, $\bar{g}$, of 8.4 m s^{-1}. We note that the Rayleigh distribution is not symmetric and requires a different interpretation than the gaussian model, which completely specifies the sample distribution by the mean and standard deviation. Nevertheless, $\bar{s}$ and σ_s are classical measures of station climatology. The seasonal cycle of the mean and standard deviation of surface wind speed at 10 m and geostrophic wind speed are shown in Fig. 4 and listed in Table 1a for the North Pole and arctic buoy data sets. Note there is little seasonal variability in s but there is a decrease in g during the summer months (top curve).

A hand anemometer was used to measure surface winds during the three and a half years (1893–1896) that the *Fram* was beset in the drifting ice pack. Mohn (1905) tabulated the monthly mean wind speed during the expedition and concluded that they do not show any regular annual period. Sverdrup (1933) observed 6-m and 500-m winds from the *Maud* as she was beset in the ice pack. The 500-m winds were estimated by tracking pilot balloons with a theodolite. Sverdrup tabulated the seasonal cycle of the monthly mean 6-m wind speed and the mean 500-m wind speed (Fig. 83, Sverdrup, 1933); the overall mean 6-m wind speed was 4 m s^{-1}, with little seasonal variation. The 500-m wind speed was about 10 m s^{-1} during the winter (November through February) and reached a minimum of 7 m s^{-1} in May, consistent with Fig. 4, nearly constant mean surface winds from summer to winter and a minimum in upper level winds in summer. Thus, the stronger

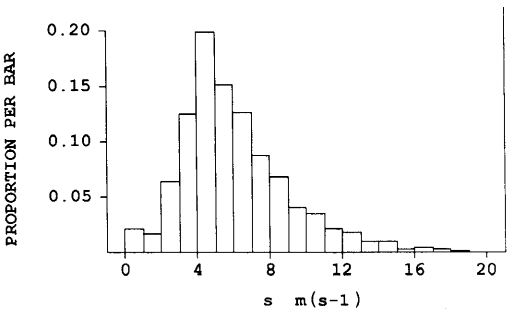

Fig. 3. Distribution of the January surface wind speed, s.

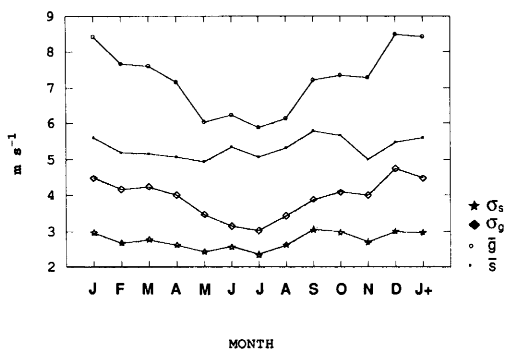

Fig. 4. Seasonal cycle of the mean monthly geostrophic wind speed, g (top curve), and surface wind speed, s, and monthly standard deviations of s and g (bottom two curves).

geostrophic winds in winter occur during periods of stronger stable stratification of the lower atmosphere, which produces the small annual variability in mean monthly surface wind speed.

4. The wind speed ratio and inflow angle

Fig. 5 shows a scatter plot of geostrophic wind speed, $g = |G|$, versus surface wind speed, $s = |w|$, for 1361 days in January. The distribution of the speed ratio $a = s/g$ is shown in Fig. 6. The distribution of the angle between the geostrophic wind and surface wind, α, is also shown in Fig. 6 for January. Note that the central part of the distribution of α is nearly gaussian but there are wide but small tails. The distribution for α is broader from the North Pole stations and arctic buoy array in Fig. 6 than in Fig. 1, where the sea level pressure measurements during CEAREX were within 50 km of the wind observation site.

The seasonal cycle of the median speed ratio a, and mean and median turning angle α, is shown in Fig. 7 and given in Tables 1a, b. In computing statistics in Table 1b we have included only cases of $s > 3$ m s^{-1} and $g > 5$ m s^{-1}. We note a narrower range between quartiles in Table 1b compared to Table 1a. For example, in January the separation between quartiles for the speed ratio is 0.39 with the full data set and 0.26 with the reduced set with a small change in the median of 0.03. For comparisons and Fig. 7, we shall use the values from Table 1b. In Tables 1a, b and Fig. 7, we also list the regression coefficient relating s to g for the 12 monthly periods. Because we expect considerably larger measurement error in estimating

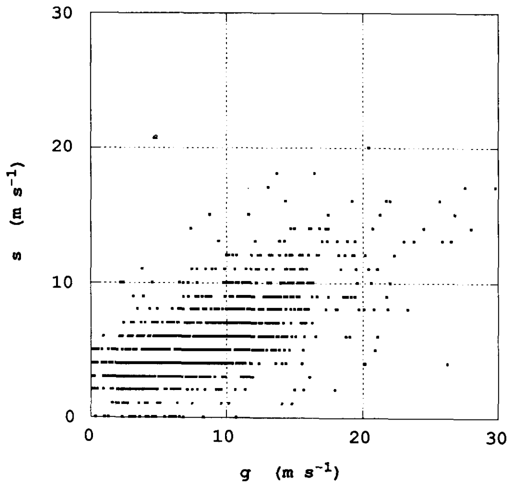

Fig. 5. Plot of the January surface wind speed versus the geostrophic wind speed.

Table 1a. *Yearly cycle of wind speed, s, geostrophic wind speed, g, reduction factor, s/g, and inflow angle, α*

		Jan.	Feb.	Mar.	Apr.	May	Jun.	Jul.	Aug.	Sep.	Oct.	Nov.	Dec.
Cases		1361	1296	1344	1200	1178	1198	1415	1302	1259	1426	1380	1469
s	median	5.0	5.0	5.0	5.0	5.0	5.0	5.0	5.0	5.0	5.0	5.0	5.0
(m/s)	mean	5.6	5.2	5.2	5.1	4.9	5.3	5.0	5.3	5.8	5.7	5.0	5.5
	σ_s	3.0	2.7	2.8	2.6	2.4	2.6	2.3	2.6	3.0	3.0	2.7	3.0
g	median	7.9	7.2	7.0	6.7	5.5	5.9	5.6	5.6	6.8	6.8	6.7	6.7
(m/s)	mean	8.4	7.7	7.6	7.1	6.1	6.2	5.8	6.1	7.2	7.3	7.3	8.5
	σ_g	4.7	4.2	4.2	4.0	3.5	3.2	3.0	3.4	3.9	4.1	4.0	4.7
s/g	median	0.67	0.68	0.68	0.72	0.83	0.84	0.85	0.88	0.79	0.78	0.66	0.64
	quartiles	0.51	0.51	0.50	0.51	0.62	0.65	0.65	0.64	0.58	0.59	0.48	0.48
		0.90	0.93	0.94	1.00	1.16	1.33	1.16	1.22	1.12	1.05	0.97	0.88
regression s/g		0.71	0.72	0.73	0.76	0.85	0.90	0.90	0.91	0.88	0.82	0.75	0.70
α	mean	33.0	34.8	34.0	37.5	22.7	21.5	26.3	21.3	26.3	31.6	32.0	31.9
(°)	median	34.7	35.8	32.7	35.2	23.7	21.8	26.8	22.7	28.9	31.7	35.1	35.2
	quartiles	10.9	11.5	15.1	16.4	1.9	1.8	4.4	1.8	2.9	10.0	9.1	12.9
		55.9	58.2	50.8	55.6	44.3	41.0	47.1	42.9	49.4	54.3	59.0	58.7

Table 1b. *Yearly cycle of reduction factor, s/g, and inflow angle, α, including only cases with $s > 3$ m s^{-1} and $g > 5$ m s^{-1}*

		Jan.	Feb.	Mar.	Apr.	May	Jun.	Jul.	Aug.	Sep.	Oct.	Nov.	Dec.
Cases		890	765	794	659	582	666	745	662	744	855	764	942
s/g	median	0.64	0.66	0.66	0.68	0.76	0.80	0.77	0.80	0.75	0.75	0.65	0.63
	quartiles	0.52	0.53	0.53	0.55	0.62	0.68	0.65	0.65	0.61	0.61	0.53	0.51
		0.78	0.81	0.81	0.84	0.92	0.97	0.95	0.98	0.96	0.92	0.80	0.79
regression s/g		0.68	0.69	0.70	0.71	0.78	0.85	0.83	0.84	0.82	0.78	0.70	0.67
α	mean	31.3	33.5	32.4	34.6	23.4	23.7	26.0	24.3	24.5	29.1	33.5	28.4
(°)	median	33.9	35.3	32.8	33.1	24.0	23.6	27.4	24.3	28.4	29.9	35.8	32.9
	quartiles	13.9	17.5	19.7	19.1	9.5	8.9	10.8	9.2	8.4	12.2	16.7	15.9
		49.3	51.8	45.6	48.1	38.1	37.5	42.8	39.8	44.5	48.0	54.9	50.9

the geostrophic wind at the ice stations than in the observed surface wind, the analysis is performed by assuming no error in the surface wind and estimating the slope of the regression line without a constant, by minimizing the error in geostrophic wind (Overland and Gemmil, 1977). The empirical results are qualitatively in agreement with observations of strongly stratified boundary layers during the winter and more neutrally stratified boundary layers in the summer. The AIDJEX data (Albright, 1980) found a summer (July through mid September) turning angle of 24° and a winter (December through mid March) angle of 30°. The AIDJEX summer angle is in good agreement with the North Pole station value of 24° for June, July and August, but the North Pole station's winter value (November–March) of 34° is greater than the AIDJEX value.

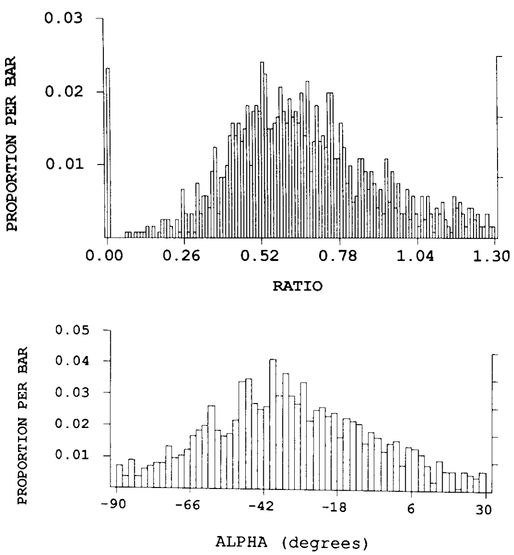

Fig. 6. Distribution of the January wind speed ratio $a = s/g$ and the inflow angle, α, between the surface and geostrophic winds.

5. Winter stability conditions

In the analysis of Overland and Davidson (1992), the parameter used to correct the geostrophic drag coefficient for stability is based on the difference between the surface temperature and that at 900 mb. The 900 mb level was chosen because it was near the base of the temperature maximum layer and at the top of the inversion layer. Many of the North Pole soundings report the pressure and temperature at the base of the temperature maximum layer as a significant level, which was generally near 900 mb. Thus we calculate the stability frequency, N_{900}, as

$$N_{900}^2 = (g/\bar{\theta})(\Delta\theta/h_{\mathrm{sig}}),$$
$$\Delta\theta = \theta_{\mathrm{sig}} - \theta_{\mathrm{s}}, \qquad \bar{\theta} = (\theta_{\mathrm{sig}} + \theta_{\mathrm{s}})/2, \tag{4}$$
$$h_{\mathrm{sig}} = 67.4\bar{\theta}\log_{10}(P_{\mathrm{s}}/P_{\mathrm{sig}}),$$

where θ_{sig} and θ_{s} are the significant level temperature and surface temperature and P_{sig} and P_{s} are the corresponding pressure.

The following procedure is used to obtain P_{sig} and θ_{sig}. If the reported level was between 880 and

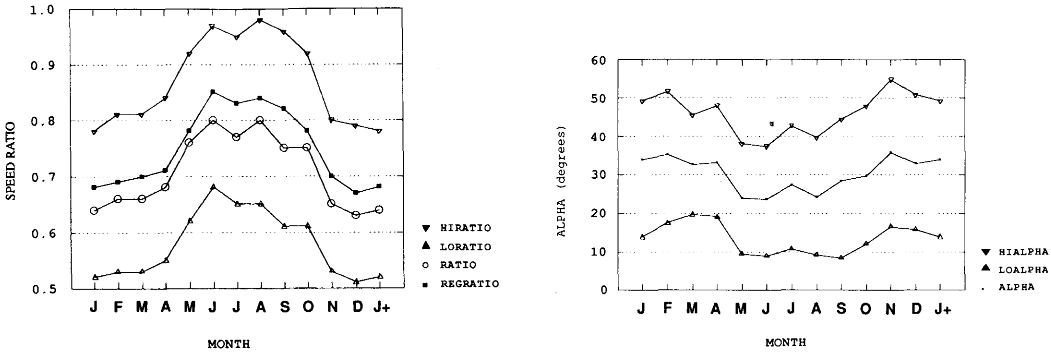

Fig. 7. (a) Annual cycle of the monthly median speed ratio and the monthly upper and lower quartile values. Also shown is the regression determined speed ratio, REGRATIO. (b) Annual cycle of the monthly median inflow angles, the upper and lower quartile values, and the mean monthly value.

925 mb, this value was used. If there was more than one report, the closest value to 900 mb was selected. If the pressure was greater than 900 mb the temperature was assigned to 900 mb, as being in the temperature maximum layer. If there was a report between 925 and 960 mb, this temperature was interpolated to the 900 mb level using reports above and below the 900 mb level. If there were no reports between 960 mb and 880 mb, then a report between 879 and 850 mb level is used. Values at 850 mb were always reported as they are a mandatory level. Because we use potential temperatures and are interested in the vertical gradient, N_{900}, the use of the 850 mb temperature in the latter case should be a reasonable approximation for the base of the temperature maximum layer.

The winter geostrophic drag coefficient and inflow angle, as a function of N_{900}, are (Overland and Davidson, 1992)

$$C_g = 0.037 - 8.3 \times 10^{-3} \left(\frac{N_{900}}{\bar{N}_{900}}\right)^4,$$

$$\bar{N}_{900} = 0.024\ \mathrm{s}^{-1}, \tag{5}$$

$$-\alpha = 11.7 + 13.1 \left(\frac{N_{900}}{\bar{N}_{900}}\right)^2. \tag{6}$$

The distribution of geostrophic drag coefficient and inflow angle for the winter central Arctic computed from eqs. (5–6) using N_{900} from three North Pole stations given in Table 2. These distributions can be compared to the observed distribution from the fall CEAREX data set (Fig. 1). The median winter geostrophic drag coefficient is 0.023 and the median inflow angle is 29° for the North Pole data set. This compares to 0.029 and 25° for the November CEAREX data set and represents a 37% lower median value in the ratio of stress to geostrophic wind squared. This is a result of the North Pole climatology being more stable with a median $N_{900} = 0.027\ \mathrm{s}^{-1}$ compared to the CEAREX median of $0.024\ \mathrm{s}^{-1}$. A value of $C_g = 0.023$ falls at the lower quartile of the distribution of the CEAREX data, and an inflow of 29° is within one quartile of the median, so that these medians based on eqs. (5–6) are not too far an extrapolation from the original CEAREX data set. The difference in median N_{900} between the

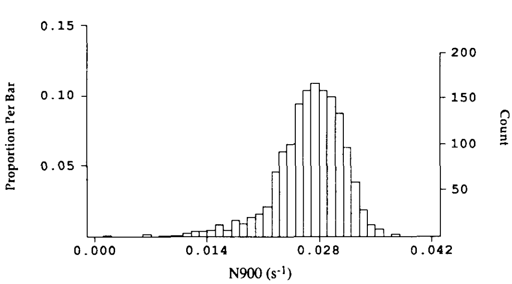

Fig. 8. Distribution of boundary layer stability, N_{900} (eq. (4)), for the winter period, November–April, as measured by NP-22, NP-26 and NP-28.

Table 2. *Summary of distribution statistics based on 1532 data points for winter months, November–April; density is $\rho = 1.47\ kg\ m^{-3}$*

	N (s^{-1})	C_g	ρC_g^2 (nt m^{-2})($m^2\ s^{-2}$)$^{-1}$	α (°)	T_s (°C)	$\Delta\theta$ (°C)
lower quartile	0.0246	0.0278	1.11×10^{-3}	−25.5	−25.1	14.9
median	0.0273	0.0232	0.79×10^{-3}	−28.6	−30.1	19.1
upper quartile	0.0297	0.0176	0.46×10^{-3}	−31.7	−35.1	23.4

CEAREX and the North Pole sites is consistent with the view that the CEAREX site is more likely to experience lower stability conditions associated with extra-tropical lows than the western Arctic.

Fig. 8 shows the distribution of the inversion layer stability, N_{900}. The quartile values are given in Table 2 along with the corresponding values of C_g, ρC_g^2 and α. 50% of the winter observations of ρC_g^2 value between 0.46×10^{-3} and 1.11×10^{-3} (n m^{-2})($m^2\ s^{-2}$)$^{-1}$. Although there is a high correlation between daily averaged geostrophic wind and ice drift (Thorndike and Colony, 1982), the ratio of wind stress to geostrophic wind speed squared can vary by $\pm 40\%$ based on the difference between the quartile values of stability. It is not clear how this stability correction can be included on a routine or historical basis, because direct observations are sparse. The use of TOVS atmospheric sounding data over the arctic ice pack has possibilities (Francis, personal communication) or perhaps operational numerical prediction models can be evaluated to see how well they analyze the gross static stability, N_{900}.

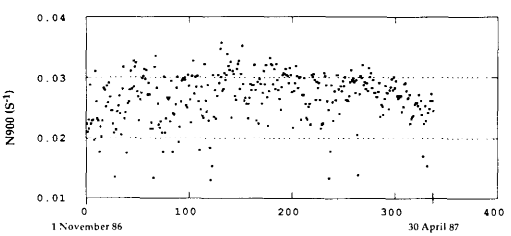

Fig. 9. Time series of boundary layer stability beginning 1 November 1986 through 31 May 1987. There is little indication of a seasonal trend throughout the 6-month winter period.

The twice daily time series of atmospheric stability, N_{900}, from the North Pole data set is shown in Fig. 9. Although there is some indication that the most stable cases occur in the first half of the winter, it does not appear straightforward to assign a more refined seasonal cycle to N_{900} or thus to C_g and α. This is in accord with the lack of within-season variability of the speed ratio or inflow angle in the Soviet drifting station surface data (Table 1b, Fig. 10).

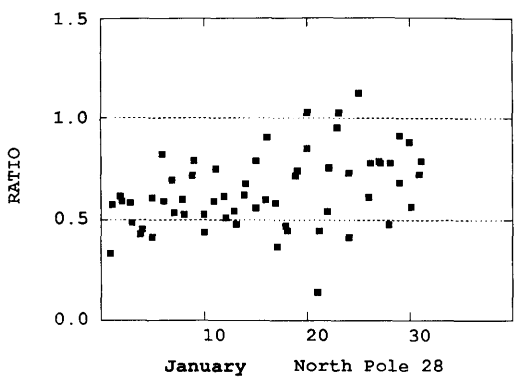

Fig. 10. Twice daily values of the speed ratio for January 1988.

6. Summer stability conditions

The arguments of the previous sections are based on the premise that the winter arctic boundary layer is primarily a radiational boundary layer with the inversion maintained by the radiative equilibrium between cold snow surface and the temperature maximum layer (Overland and Guest, 1991). During the summer months the radiative balance at the surface is reversed due to solar heating (Maykut, 1986). Surface temperatures (June–August) remain near the melting point with a median temperature of −0.5° and a difference of 2.3° between quartiles. The summer is dominated by elevated inversions (Serreze et al.,

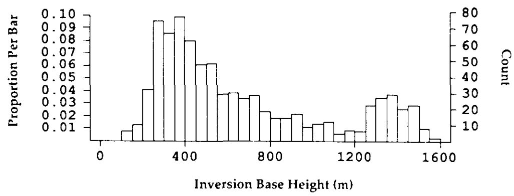

Fig. 11. Distribution of inversion base heights with a mode near 350 m in accord with Serreze et al. (1992). The secondary maximum near 1300 m are those soundings with no inversion base below 850 mb.

1992; Fig. 7). Fig. 11 shows the distribution of the inversion base from the North Pole data set with a mode between 350 and 400 m.

Overland (1985) developed a second-order closure atmospheric model to estimate the value of C_g and α in the presence of an elevated inversion (Overland and Davidson, 1992, Fig. 3). Using the median windspeed of $5.0\,\mathrm{m\,s^{-1}}$ from the summer North Pole data set, an inversion base height, Z_i, of 350 m (Fig. 11), a summer surface roughness 10 m drag coefficient of 2.2×10^{-3} (Overland, 1985), and a Coriolis parameter of $1.46 \times 10^{-4}\,\mathrm{s^{-1}}$, yields a value of $u_*(fZ_i)^{-1}$ of 5, which is well within the range of near-neutral stability and predicts values of $C_g \approx 0.032$ and $-\alpha \approx 15°$. If we use eqs. (5–6) with the median $N_{\mathrm{base}} = 0.0136\,\mathrm{s^{-1}}$, then $C_g = 0.036$ and $-\alpha = 15.9°$. Possible summer values for the central Arctic based on temperature sounding data are $C_g = 0.033$, $-\alpha = 15°$, $\rho = 1.29\,\mathrm{kg\,m^{-3}}$ and $\rho C_g^2 = 1.4 \times 10^{-3}\,(\mathrm{n\,m^{-2}})(\mathrm{m^2\,s^{-2}})^{-1}$.

7. Discussion and composite results

Comparison of inflow angles and geostrophic drag coefficients by different methods and data sets are summarized in Table 3. To convert a speed ratio to a geostrophic drag coefficient we need a surface layer 10-m drag coefficient, C_{10},

$$C_g = C_{10}^{1/2} s/g. \tag{7}$$

Here, C_{10} represents a regional value of air-ice coupling which includes the influence of ridges and leads. The values of C_{10} collected from before 1984 were reviewed by Overland (1985); a winter value of C_{10} ranges from 1.9×10^{-3} to 2.6×10^{-3} (Overland, 1985; Walter and Overland, personal communication) while a single observation for summer is 2.2×10^{-3}. The regional value used for the fall CEAREX site was 2.5×10^{-3}. We shall use a value of 2.2×10^{-3} for both summer and winter. Central arctic values for different ice types may differ by $\pm 20\%$ from the 2.2×10^{-3} value, but their influence on C_g through eq. (7) is at most $\sim 9\%$. While there are considerable measurements of C_{10} for the marginal ice zone (Guest and Davidson, 1991), there are, unfortunately, few regional coefficients for the central Arctic.

The values based on the soviet station/drifting buoy array are larger than those from AIDJEX and CEAREX, $a \sim 0.65$–0.69 compared to $a \sim 0.49$–0.55 for winter. This is a major difference. In AIDJEX and CEAREX gradients of sea-level pressure are estimated from stations 100 km apart or less. Two possibilities are that estimates of stronger pressure gradients are underestimated by the Arctic buoy array because the spacing is large (500–600 km) and of the same size as the weather systems themselves, or that the difference is due to smoothing in the analyses and interpolation schemes. We thus recommend a factor, γ,

$$\tau = \rho C_g^2 \gamma^2 g^2, \tag{8}$$

when the spacing of the sea level pressure

Table 3. *Comparison of methods*

	Winter (November–March)			Summer (June–August)		
	s/g	γC_g	α	s/g	γC_g	α
NP surface data (sort)	0.65	0.030[a]	34	0.79	0.037[a]	25
NP surface data (regression)	0.69	0.032[a]	—	0.84	0.039[a]	—
CEAREX model (NP soundings)	0.49	0.023	29	0.70	0.033	15+
AIDJEX (Albright, 1980)	0.55	0.026	30	0.60	0.028	24
AIDJEX (Carsey, 1980)	0.55	0.023	29	0.62	0.026	24

[a] For these cases we assume that $\gamma \approx 1.3$.

measurements is greater than 400 km, such as in the arctic buoy array. From Table 3, we take a value of $\gamma = 1.3$; this is obtained by dividing the average of the top two numbers of γC_g in Table 3 for winter and summer by the average of the bottom three numbers. Thus we recommend keeping C_g as a regional scale, 40–100 km, value based on AIDJEX and CEAREX, and adjust the estimate of the local geostrophic wind for the arctic buoy array through the use of the factor γ. For winter we recommend $C_g \sim 0.024$ and $\rho C_g^2 \sim 0.85 \times 10^{-3}$ $(\text{n m}^{-2})(\text{m}^2\,\text{s}^{-2})^{-1}$ and for summer $C_g \sim 0.029$ with $\rho C_g^2 \sim 1.10 \times 10^{-3}$ $(\text{n m}^{-2})(\text{m}^2\,\text{s}^{-2})^{-1}$. Thus the North Pole surface wind speed data is not used to provide an independent estimate of C_g, but to provide the calibration factor γ for estimating the local geostrophic wind from the arctic buoy program. It is unclear what value of γ to use with the NMC or Fleet Numerical gridded sea level pressures; γ ought to lie between 1.0 and 1.3.

The difference in inflow angles between AIDJEX/CEAREX and Soviet North Pole stations are more problematic. The CEAREX summer values based on a model may be low because there may be some weak stable stability to the summer boundary layer; an α value of 20° is not inconsistent. Summer values then range 20–24° and winter values are 29–34°; we recommend 23° for summer and 33° for winter, relying primarily on the North Pole data set.

8. Evaluation of the Overland and Davidson (1992) model against North Pole station data

Because we consider that the speed ratio provides the primary determination of C_g, we can test the variance of the Overland and Davidson (1992) predictions for C_g based on atmospheric stability against the variance of the speed ratios provided at the North Pole stations. We test the model

$$\frac{s}{g} = f(N_{900}^4) \tag{9}$$

in the form

$$\ln s = d \ln g + e \ln N_{900}, \tag{9'}$$

where d and e are regression coefficients. With e equal to zero, the r^2, correlation is 0.920. This is increased to an $r^2 = 0.944$ with the full model. Thus the influence of stability has provided an improvement, which is significant based on the F test at 5% for 1530 degrees of freedom. The stability dependent model has skill, although the exact amount is unclear as we have not accounted for the expected errors in g. The square correlation of s with g is 0.868.

We note that the composite value for the winter average C_g from Section 7 is near the prediction from the regression model (5), so no adjustment is needed in eq. (5). However, we have increased the inflow angle from 29° to a composite value of 33°; thus the inflow angle predicted from (6) from Overland and Davidson (1992) should be increased by 4° or

$$-\alpha = 15.7 + 13.1 \left(\frac{N_{900}}{\bar{N}_{900}}\right)^2. \tag{6'}$$

9. Conclusions

Based on 10 years of surface data and almost six complete station years of atmospheric soundings from the Soviet North Pole stations, we have established the climatology for surface winds and the stability of the radiational boundary layer for the western central Arctic. We relate this climatology to the value of geostrophic drag coefficient. The stability regression model of Overland and Davidson (1992) is validated by comparison to the North Pole station data.

For use in driving sea-ice models of the central Arctic basin we recommend

$$\begin{aligned} &\tau = \rho C_g^2 \gamma^2 g^2, \\ &\rho C_g^2 = 0.85 \times 10^{-3}\ (\text{n m}^{-2})(\text{m}^2\,\text{s}^{-2})^{-1} \\ &\quad \text{November–March}, \\ &\rho C_g^2 = 1.10 \times 10^{-3}\ (\text{n m}^{-2})(\text{m}^2\,\text{s}^{-2})^{-1} \\ &\quad \text{June–August}, \end{aligned} \tag{11}$$

with interpolation during the transition months of April, May, September and October. The factor γ equals 1.3 if the grid points used for estimating the geostrophic wind are farther apart than 400 km;

this factor is applicable to the arctic buoy program array. An inflow angle of 33° is recommended for winter and 23° for summer. With no further information on boundary layer stability, estimates based on any particular daily realization (11) may have errors of $\pm 40\%$ for any particular realization during the winter period. However, there is little variability in the monthly median values for the summer and winter periods. The daily variability of stability, N_{900}, and thus C_g and α may be available through TOV data.

10. Acknowledgments

We thank Mark Serreze for making the sounding data set available to us and acknowledge the Soviet personnel who created such an extensive and valuable data set. We also thank Ryan Whitney and Virginia Vose for manuscript preparation. This paper is a continuation of the CEAREX project which was supported by Arctic Programs and Marine Meteorology of the Office of Naval Research.

REFERENCES

Albright, M. 1980. Geostrophic wind calculations for AIDJEX. *Sea ice processes and models*, R. S. Pritchard (ed.). University of Washington Press, Seattle, pp. 62–75.

Carsey, F. D. 1980. The boundary layer height in air stress measurement. *Sea ice processes and models*, R. S. Pritchard (ed.). University of Washington Press, Seattle, pp. 443–451.

Colony, R. L. and Rigor, I. 1991. *Arctic ocean buoy program data report*, APL-UWTM 10–91. National Snow and Ice Data Center, Boulder, CO, 142 pp.

Doronin, Y. P. 1969. *Thermal interaction of the atmosphere and the hydrosphere in the Arctic*. Gidrometeorologicheskoe Izdatel'stvo, Leningrad, 224 pp.

Guest, P. S. and Davidson, K. L. 1991. The aerodynamic roughness of different types of sea ice. *J. Geophys. Res.* **96**, 4709–4722.

Kitaigorodskii, S. A. 1988. A note on similarity theory for atmospheric boundary layers in the presence of background stable stratification. *Tellus* **40A**, 434–438.

Maykut, G. A. 1986. Surface heat and mass balance. *The geophysics of sea ice*, N. Untersteiner (ed.). NATO ASI Series, Series B, vol. 46, Plenum Press. New York, 395–463.

Mohn, H. 1905. Meteorology. *The Norwegian north polar expedition 1893–1896, Scientific Results*, vol. 6, F. Nansen (ed.). Greenwood Press, New York, 697 pp.

Overland, J. E. 1985. Atmospheric boundary layer structure and drag coefficients over sea ice. *J. Geophys. Res.* **90**, 9029–9049.

Overland, J. E. and Davidson, K. L. 1992. Geostrophic drag coefficients over sea ice. *Tellus* **44A**, 54–66.

Overland, J. E. and Gemmill, W. H. 1977. Prediction of marine winds in the New York Bight. *Mon. Weather Rev.* **105**, 1003–1008.

Overland, J. E. and Guest, P. S. 1991. Control of minimum snow and air temperature over arctic sea ice during winter. *J. Geophys. Res.* **96**, 4651–4662.

Serreze, M. C., Kahl, J. D. and Schnell, R. C. 1992. Low-level temperature inversions of the Eurasian Arctic and comparisons with Soviet drifting station data. *J. Climate* **5**, 615–629.

Sverdrup, H. U. 1933. General report of the expedition. *The Norwegian north polar expedition with the "Maud" 1918–1925, scientific results*, vol. 1, No. 1. Geofysisk Institutt, Bergen.

Thorndike, A. S. and Colony, R. 1982. Sea ice motion in response to geostrophic winds. *J. Geophys. Res.* **89**, 5845–5852.

Thorndike, A. S., Colony, R. and Munoz, E. A. 1983. *Arctic ocean buoy program: data report, 1 January 1982–31 December 1982*. Applied Physics Laboratory, University of Washington, Seattle, 132 pp.

Walter, B. A. and Overland, J. E. 1991. Aircraft observations of the mean and turbulent structure of the atmospheric boundary layer during spring in the central Arctic. *J. Geophys. Res.* **96**, 4663–4674.